

Experimental Study of under-platform Damper Kinematics in Presence of Blade Dynamics

D Botto, C Gastaldi, M M Gola and M Umer¹

DIMEAS Politecnico di Torino, Italy

¹Corresponding author: muhammad.umer@polito.it

Abstract. Among the different devices used in the aerospace industries under-platform dampers are widely used in turbo engines to mitigate the blade vibration. Nevertheless, the damper behaviour is not easy to simulate and engineers have been working in order to improve the accuracy with which theoretical contact models predict the damper behaviour. Majority of the experimental setups collect experimental data in terms of blade amplitude reduction which do not increase the knowledge about the damper dynamics and therefore the uncertainty on the damper behaviour remains a big issue. In this paper, a novel test rig has been purposely designed to accommodate a single blade and two under-platform dampers to deeply investigate the damper-blade interactions. In this test bench, a contact force measuring system was designed to extensively measure the damper contact forces. Damper kinematics is rebuilt by using the relative displacement measured between damper and blade. This paper describes the concept behind the new approach, shows the details of new test rig and discusses experimental results by comparing with previously measured results on an old experimental setup.

1. Introduction

Some test rigs [1- 4] were developed in the past to mainly study the overall effect of the dampers on the blade in terms of vibration amplitude reduction and resonant frequency shift. These test rigs do not provide facility to analyse in depth the dynamics of the damper and its kinematics in terms damper/under-platform relative displacement. The effect of the dampers on the blade dynamics can be studied by introducing the two contact parameters known as normal and tangential contact stiffness. In [5] a method has been proposed to determine the contact stiffnesses of complex contact geometries. Test rigs were developed in [6 , 7] and used to measure the friction coefficient and the tangential contact stiffness, in controlled laboratory conditions. A Damper Rig [8] was built in 2008 to deeply investigate the behaviour of several dampers in terms of kinematics and force transmission characteristics [9, 10]. A numerical model of the damper/test-rig system was presented in [11], together with the first version of the contact parameters estimation procedure, subsequently improved in [12]. The Damper+Blade Rig presented here in this paper share with the Damper Rig the same ultimate goal: measuring the hysteresis cycle produced by the damper between the platforms. However, their structure and working principles are different. In the first rig (Damper Rig) the trajectory and amplitude of the input motion can be finely controlled by means of two piezo actuators connected to a dummy platform (no blades are present). However, the frequency range, the rig can explore is limited (lower than 160 Hz). In the second rig, (see section 2) the motion is achieved by exciting a blade at resonance; therefore, the variety of platform kinematics the user can investigate are limited. However, the rig is excited in the frequency range actually encountered by the blades during



working. Furthermore, in this second rig it is possible to directly measure the effect of the damper hysteresis cycle on the blade amplitude of vibration. These two test rigs have complementary capabilities. Furthermore, they offer the possibility to test the same dampers, compare the resulting performance in terms of hysteresis cycles, and contact parameters. Section 4 contains such a comparison for the pre-optimized damper geometry presented in [12].

2. Test Rig Description

Figure 1 shows the top view, a section and details of the rig. The test rig is composed of three main sub-assemblies, namely a central block and two lateral blocks. The central block is made of two symmetric parts, (1A) and (1B). The two symmetric parts are fixed to an optical table through a base plate (2) with 32 vertical bolts. The two parts house a clamping mechanism. The clamping mechanism applies the centrifugal load on the blade. This clamping mechanism is made of two wedge blocks (3) and (4), with a slope of 1:10. These wedges convert a force F_B applied by main bolt (5) perpendicular to the longitudinal axis of the blade into a pushing force F_P acting along the longitudinal axis. Due to the 1:10 slope between the two wedges, the nominal force amplification A_{nom} between the bolt force F_B and the pushing force F_P is 10. A strain gages based load cell (6) measures the applied bolt force F_B . A thrust ball bearing (7) is placed between the main bolt and the load cell to allow their relative rotation. The subassembly composed of the main bolt, the thrust ball bearing and the load cell is enclosed in a casing (8) tightened to the central block with screws. Two rails of linear flat roller bearings (9) are introduced between the moving contact surfaces of wedge blocks to minimize the friction losses. The pushing force F_P is transmitted to the blade (11) through the pushing block (12). Between the pushing block and the upper wedge an aligning pin (13) allows small rotation between the upper wedge and the pushing block. The aligning pin allows to apply a uniform pressure at the blade root even if a small misalignment is present between the blade and the upper wedge. To avoid damage due to the high contact pressure, the self-aligning pin and its counterparts on the pushing block and the upper wedge have been designed with conforming contact surfaces. Pressure distribution on conforming contact surfaces has been deduced by the graphs found in [13]. The blade is inserted in the blade adapter (14) in which a bucket groove has been machined to match the blade root geometry. The blade adapter is pushed against the shoulders on the central block. As the blade adapter is a replaceable part, blades with a different root can be tested by simply changing the adapter according to any blade root geometry. Eight long stud bolts are inserted across the two parts of the central block, by means of through-holes (15), to hold the complete assembly altogether and stiffen the structure. These stud bolts co-operate with the vertical bolts to increase the rigidity of the overall structure. A complete description of this test rig is present in [14].

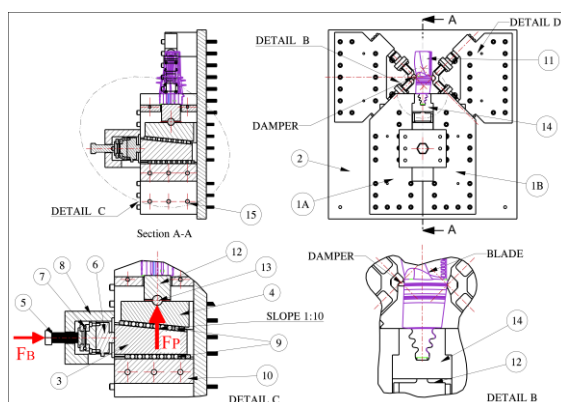


Figure 1. Test rig assembly details with a real turbine blade and two dampers.

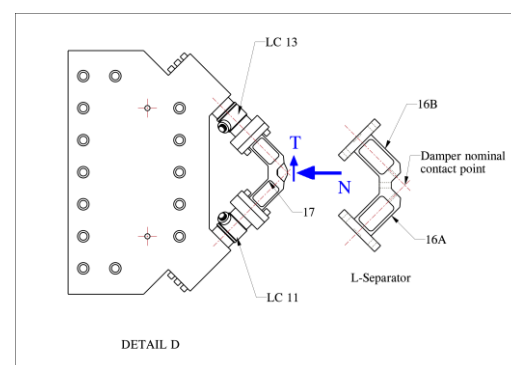


Figure 2. Contact force measuring system used to contact forces on one side of the damper.

Measuring the contact forces acting on the both dampers is a significant feature of this novel test rig. Two contact force measuring devices, one for each damper, are available to measure their

respective force components. A device is shown in figure 2 that has a two arms structure (16A and 16B) named L-Separator. The axes of the two arms are oriented at 90° to each other which intersect at the point of nominal contact between the damper and the pad. Two piezoelectric load cells LC (LC_{11} , LC_{13}) are coaxially mounted at the other end of both arms. The ratio between the longitudinal and transverse stiffness is around 100 to neglect any transverse force component. The contact forces N and T are deduced by the signals measured by each load cell. The selected load cells are able to measure both static and dynamic force component due to very low time drift factor (i.e. lower than 5 mN/s).

3. Experimental Procedure:

Experimental tests were performed on a dummy blade with a fir-tree root clamped with a constant pushing force of 50kN, a realistic value for similar blades in real turbine. Tests were carried out with different blade excitations at several centrifugal loads applied to the dampers in form of dead weights. For each testing condition a standard force-controlled Frequency Response Function (FRF) was obtained in which acceleration at the tip of the blade was measured. As FRFs alone do not give an insight into the damper behaviour, the present test rig is capable of linking a given point on a FRF to the corresponding damper-platform contact forces and relative displacements. In the following paragraph, all measured and reconstructed quantities are described. This set of quantities will then be used in section 4 to analyse the dampers and the blade behaviour together with their mutual influence.

The readings of the contact force measuring load cells mentioned in section 2 and shown in figure 2 give the complete in-plane force components at the cylindrical side of the dampers. As already mentioned the measurement chain composed of load cell and a charge amplifier allows measuring the static component of forces as well as their dynamic variation. The static components are necessary to reconstruct the damper equilibrium and to estimate friction coefficients. The tangential and normal to the contact force components, here termed T_{cyl} and N_{cyl} are computed from measured forces (F_{12} and F_{14} , F_{11} and F_{13}). Furthermore, the damper static equilibrium is reconstructed by neglecting damper mass inertia forces (lower than 0.1 N in the frequency range of interest) and therefore assuming contact and centrifugal forces to pass through one point, as described in [10] and shown in figure 3. The relative displacements at the damper platforms are measured by using a differential laser head. A complete set up of the test rig to measure the damper contact forces and relative displacement is shown in figure 4. These displacements are plotted against the tangential component of corresponding contact force to obtain the hysteresis loops. Hysteresis loops are commonly used to describe the characteristics of the frictional contacts. An example of these hysteresis with corresponding FRFs can be seen in figure 5.

4. Results and discussion

As shown in figure 6a the damper shifts the first bending mode resonant frequency from 410 Hz to 567.5 Hz in full stick condition ($|F_E|=1N$) and lowers the force-normalized blade amplitude of motion of one order of magnitude. This effect is produced by the dampers, which start to slip against the platforms and dissipate energy, therefore reducing the amplitude of the FRF peak and reduces the stiffness introduced by the contact in full stick. Details of all these experiments and methodology is discussed in [15].

4.1. Measured contact hysteresis loops explain puzzling measured FRFs

A general understanding of the damper effect on the blades is nowadays common knowledge in the turbine dynamics field. However, there are still a series of open questions which turbine designers and experimenters face. The first question is related to the experimental characterization of damper-blades systems. FRFs sometimes produce unexpected results which are hard to understand and justify. For instance, with reference to figure 6a and figure 7, it can be noticed how the amplitude and the frequency of the peak decreases for $|F_E|$ ranging from 1 N to 50 N, as expected. However, for $|F_E| \geq 80$ N the peak amplitude and frequency start increasing again. This behaviour is repeatable, and is observed at different loads on the damper. Without an insight on the damper behaviour this

phenomenon would remain unexplained. Thanks to the test rig capabilities it is now possible to relate the FRF shape to the corresponding damper behaviour. Figure 6b shows the hysteresis cycle at the cylindrical contact for two different values of $|F_E|$ (50 N and 100 N respectively). It can be seen that at $|F_E|=50$ N the cylindrical interface is in micro-slip/at the onset of gross slip: this behaviour is easily simulated with the numerical code by considering the blade platform as rigid body. At $|F_E|=100$ N the contact is slipping and therefore dissipating energy, however during part of the cycle the damper appears to be “glued” to the platform. Specifically the tangential force changes its value but no relative movement between damper and platform is recorded. This behaviour introduces an additional stiffness to the system, thus producing an increase of the peak frequency.

Another experimental observation which puzzles designers during testing is the marked lack of repeatability for the same test conditions. The results reported in figure 6a and figure 7 are obtained starting from $|F_E|=1$ N and going up to $|F_E|=100$ N. If the same set of experiments is repeated, without unloading the dampers, in the opposite order (from $|F_E|=100$ N to 1N) the FRFs obtained in the micro-slip region ($|F_E|\leq 20$ N) will be markedly different from the first set. An example can be found in figure 5. The results of several test campaigns are reported in figure 5a to show that the results are not randomly distributed. They are in-fact quite repeatable, provided that the initial conditions are the same. In the micro-slip regime, the steady state solution is non-unique; it depends on the initial conditions, namely the value of the static component of contact forces as pointed out also by the Yang and Menq in [16]. More recently these authors showed in [17] that using the damper static balance equations to compute the normal preloads acting on the damper sides does not allow calculating a unique solution if the contact is partially stuck. These authors numerically demonstrated the effect of this under-determinacy on under-platform dampers in [10]. Using the test rig presented here, the numerical observations described above have found an experimental counterpart. By reconstructing the static equilibrium on the damper as explained in section 3, N-flat and T-flat and their point of application on the damper are determined. Figure 5c shows that the static component of the normal contact forces undergo a 50 % increase if the damper enters the gross-slip regime (i.e. if the blade is excited with $|F_E|=100$ N). This produces different steady state hysteresis cycles (figure 5b): specifically, if the static normal components of contact forces are low, the damper is in micro-slip (blue). If the normal components increase the steady state cycle will be larger (black dashed line) but the damper will also remain glued to the platform for a portion of the cycle, similarly to what was happening at $|F_E|=100$ N. The damper behaviour at the contact is perfectly compatible with the FRFs: the one corresponding to higher contact forces displays a higher peak frequency (due to the additional stiffness) and a larger amplitude.

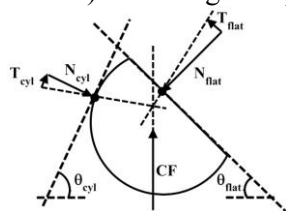


Figure 3. Damper force equilibrium.

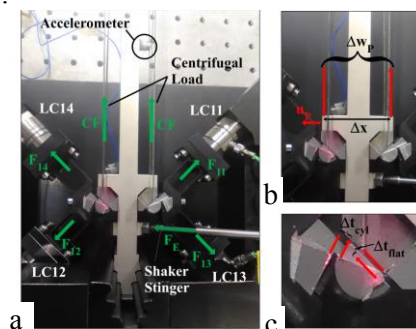


Figure 4 (a) Test rig setup, measured and applied force. (b) Laser setup to record the blade platform in-plane motion. (c) Laser setup to measure tangential relative displacement at the flat-on-flat and cylinder-on flat contacts.

4.2. Damper performance simulation

The numerical model used to simulate the damper behaviour, fully described and validated in [10], is shown in figure 8a. It represents the damper, modelled as a rigid body, between two platforms, with assigned motion. The contact is modelled through standard macro-slip elements. Inputs to the numerical model are: the platform motion signal and the friction contact parameters estimated in [18] and confirmed by the measurements in section 4.3. The resulting force equilibrium is reported in figure 8c. It compares well with the measured counterpart (see figure 8b), thus confirming the reliability of the measurements and the interpretation of experimental results.

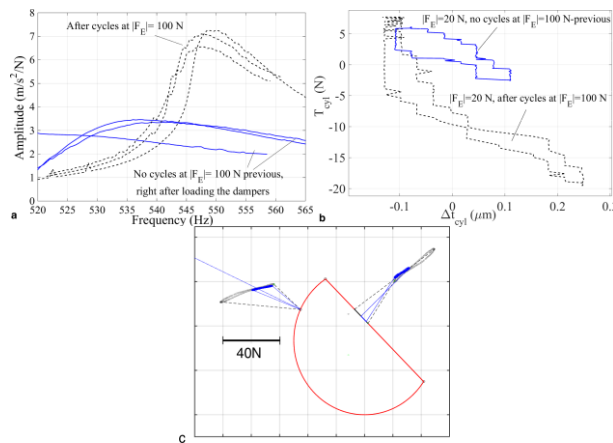


Figure 5 (a) FRFs (b) Hysteresis cycles at damper cylindrical contact (c) Equilibrium at $CF=4.6\text{kg}$ $F_E=20\text{N}$ initial condition comparison.

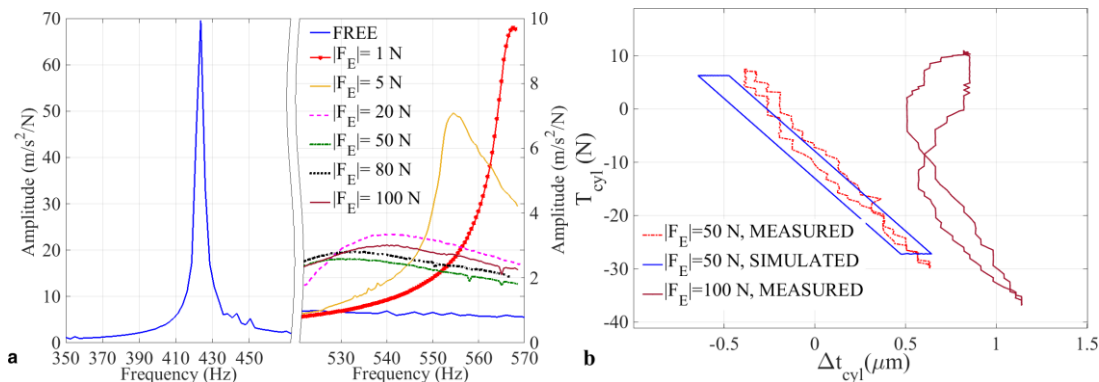
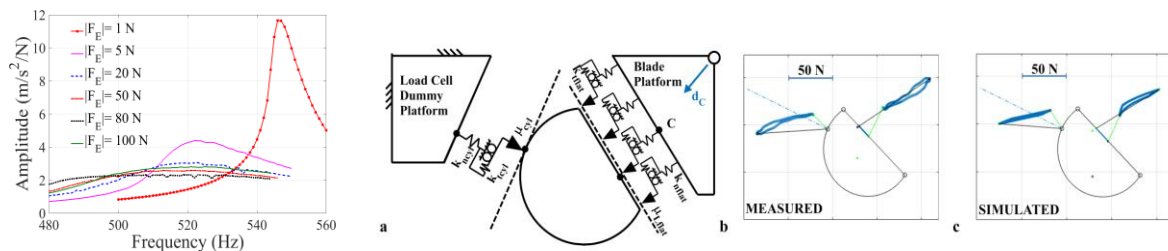
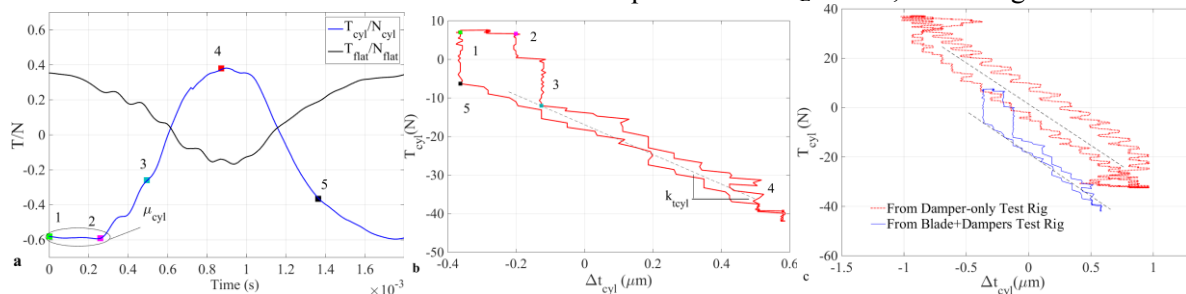


Figure 6 (a) FRF free (without dampers) and with dampers $CF= 4.6\text{kg}$ (b) Measured and simulated hysteresis at cylindrical side of the damper for working conditions shown in figure 5a.

4.3. Comparison of damper parameters and performance on two independent test rigs

To numerically validate the experimental results, these authors developed a contact parameter estimation technique in [10], further improved in [18], and based on the experimental observation of the piezo damper only test rig, specifically it was observed that; friction coefficient and contact stiffness are obtained from the ratio of tangential/normal force and corresponding slope of the hysteresis cycle respectively. The similar technique was adapted on the obtained experimental data on this novel test rig and computed results were compared with the results presented in [12] and [18] where exactly same dampers were tested. A case with $|F_E|=100\text{N}$ (similar to the one in figure 6b) has been selected in order to ensure the cylindrical contact to reach gross-slip. Specific points on the hysteresis diagram have been marked by a symbol and a number to allow a cross-comparison. From the combined analysis of the T/N diagram and of the hysteresis at the cylindrical contact in figure 9 it holds:

- from markers 1 to 2 the cylindrical contact is sliding since the T_{cyl}/N_{cyl} is constant and equal to a maximum, $\mu_{cyl}=0.6$, exactly the same value measured on the damper-only test rig [12];
- from markers 2-3 and 5-1 presents a sharp increase of tangential force with no movement and from markers 2-5 the state is stick, the measured tangential stiffness $kt_{cyl} \approx 35\text{N}/\mu\text{m} \pm 9\text{N}/\mu\text{m}$, perfectly compatible with the $30\text{N}/\mu\text{m} \pm 7\text{N}/\mu\text{m}$ measured on the damper only test rig [18].

**Figure 7** FRFs CF=2.6kg.**Figure 8(a)** Damper numerical model (b, c) Measured and simulated forced equilibrium at $F_E=100\text{N}$, CF=4.6kg.**Figure 9** (a) T/N force ratio (b) Hysteresis at $F_E=100\text{N}$, CF=4.6kg (c) Hysteresis slope comparison of cylindrical to flat contact obtained on two independent and different test rigs.

5. Conclusion

The capabilities of the novel test rig allow an insight investigation into the damper behaviour. Namely for each point on a FRF the corresponding hysteresis at the contacts, force equilibrium and platform kinematics can be produced. This set of diagrams is particularly helpful in explaining unexpected phenomena (e.g. FRFs lack of repeatability) which often makes experimental characterization of damper-blade systems difficult. The test rig can be used to estimate friction contact parameters, which compare extremely well with the values found for the same damper on an independent test rig (damper-only test rig). These findings speak for the soundness of both test rigs and for the estimation procedure itself. The obtained experimental results are compared with the results obtained on a previous reference damper-only test rig. These results comparison highlight the importance of considering the blade mode shape to achieve a full understanding of the system dynamics and as a mean to achieve a better and faster damper shape optimization.

References

- [1] Panning L, Sextro W and Popp K 2000 Optimization of inter-blade friction damper design. *In Proc. of ASME Gas Turbine & Aero engine congress and exhibition (Munich)*
- [2] Petrov E P and Ewins D J 2002 Analytical formulation of friction interface elements of nonlinear multi-harmonic vibrations of bladed discs. *In Proc. of ASME Turbo Expo (Amsterdam)*
- [3] Firrone C M 2009 Measurement of the kinematics of two under- platform dampers with different geometry and comparison with numerical simulation *J. of sound and vibration* **323** 313-33
- [4] Bessone A, Toso F and Berruti T 2015 Investigation on the dynamic response of blades with asymmetric under platform dampers. *In proc. of ASME Turbo Expo Montreal (Quebec)*
- [5] Botto D, Lavella M 2015 A numerical method to solve the normal and tangential contact problem of elastic bodies *Wear* **330-331** 629-35
- [6] Filippi S, Akay A and Gola M M 2004 Measurements of tangential contact hysteresis during micro-slip *J. of Tribology* **126** 482-89
- [7] Lavella M, Botto D and Gola M M 2013 Design of a high- precision, flat-on-flat fretting test apparatus with high temperature capability *Wear* **302** 1073-81

- [8] Gola M M, Braga dos Santos M and Liu T 2010 Design of a new test rig to evaluate under-platform damper performance *In Proc. of ESDA (Istanbul)*
- [9] Gola M M, Bragas Dos Santos M and Liu T 2012 Measurement of the scatter of under-platform damper hysteresis cycle: experimental approach. *In Proc. of ASME IDETC (Chicago)* pp 359–69
- [10] Gola M M and Gastaldi C 2014 Understanding complexities in under-platform damper mechanics *In Proc. ASME Turbo Expo (Düsseldorf)* vol.7A
- [11] Gola M M and Liu T 2014 A direct experimental-numerical method for investigations of a laboratory under-platform damper behaviour *Int. J. of Solids and Structures*. **51** 4245–59
- [12] Gastaldi C and Gola M 2016 Pre-optimization of asymmetrical under-platform dampers *J. Eng. Gas Turbines Power* **139** (1)
- [13] Johnson K L 1985 *Contact Mechanics* (Cambridge: Cambridge University Press) pp114–18
- [14] Botto D, and Umer M 2018 A novel test rig to investigate under-platform damper dynamics *Mech. Syst. Signal Proc.* **100** 344–59
- [15] Botto D, Gastaldi C, Gola M M and Umer M 2017 An experimental investigation of the dynamic of a blade with two under platform damper *J. Eng. Gas Turbines Power* **140** (3) 032504-9
- [16] Yang B D and Menq C H 1998 Characterization of contact kinematics and application to the design of wedge dampers in turbomachinery blading: Part1-stick-slip contact kinematics *J. Eng. Gas Turbines Power* **120** (1) 410–17
- [17] Zucca S, Botto D and Gola M M 2008 Range of variability in the dynamics of semi-cylindrical friction dampers for turbine blades *In Proc. of ASME Turbo Expo (Berlin)* pp 519-29
- [18] Gastaldi C and Gola M M 2016 Testing, simulating and understanding under-platform damper dynamics *In VII European Congress on Computational Methods in Applied Sciences and Engineering (Crete)*